https://doi.org/10.5194/bg-2022-245
Preprint. Discussion started: 6 January 2023
© Author(s) 2023. CC BY 4.0 License.

Biogeosciences Discussions
Open Access
EGU

Photophysiological response of autumn phytoplankton in the Antarctic Sea-Ice Zone

Asmita Singh[1,2], Susanne Fietz[1], Sandy J. Thomalla[2], Nicolas Sanchez[3], Murat V. Ardelan[3], Sébastien Moreau[4], Hanna M. Kauko[4], Agneta Fransson[4], Melissa Chierici[5], Saumik Samanta[1], Thato N. Mtshali[6], Alakendra N. Roychoudhury[1] and Thomas J. Ryan-Keogh[2]

[1] Department of Earth Sciences, University of Stellenbosch, Stellenbosch, South Africa
[2] Southern Ocean Carbon-Climate Observatory, CSIR, Cape Town, South Africa
[3] Department of Chemistry, Norwegian University of Science and Technology (NTNU), Trondheim, Norway
[4] Norwegian Polar Institute (NPI), Tromsø, Norway
[5] Institute of Marine Research, Fram Centre, Tromsø, Norway
[6] Oceans and Coast, Department of Environment, Forestry and Fisheries, Cape Town, South Africa

Correspondence to: Thomas J. Ryan-Keogh (tryankeogh@csir.co.za)

Abstract. The High Nutrient-Low Chlorophyll condition of the Southern Ocean is generally thought to be caused by the low bioavailability of micronutrients, particularly iron, which plays an integral role in phytoplankton photosynthesis. Nevertheless, the Southern Ocean experiences seasonal blooms that generally initiate in austral spring, peak in summer and extend into autumn. This seasonal increase in primary productivity is typically linked to the seasonal characteristics of nutrient and light supply. To better understand the constraints on productivity in the Antarctic Sea-Ice Zone (SIZ), the photophysiological response of phytoplankton to iron addition was investigated during autumn along the Antarctic coast off Dronning Maud Land. Five short-term (24 hr) incubation experiments were conducted around Astrid Ridge (68°S) and along a 6°E transect, where an autumn bloom was identified in the region of the western SIZ. Surface iron concentrations ranged from 0.27 to 1.39 nM around Astrid Ridge, and 0.56 to 0.63 nM along the 6°E transect. The photophysiological response of phytoplankton to iron addition, measured through the photosynthetic efficiency and the absorption cross-section for photosystem II, showed no significant responses. This confirms that phytoplankton were not iron-limited at the time and that ambient iron concentrations were sufficient to fulfil the cellular requirements. This provides new insights into extended iron replete post-bloom conditions in the typically assumed iron deficient High Nutrient-Low Chlorophyll Southern Ocean.

https://doi.org/10.5194/bg-2022-245
Preprint. Discussion started: 6 January 2023
© Author(s) 2023. CC BY 4.0 License.

1 Introduction

The Southern Ocean plays an important role in the global drawdown of atmospheric carbon dioxide (CO_2) (Khatiwala et al., 2009; Takahashi et al., 2002; 2009), which is partially driven by the biological carbon pump through phytoplankton photosynthetic carbon uptake and export. Seasonal changes in the physical and chemical environment of the Southern Ocean are expected to modify the physiological (Deppeler and Davidson 2017; Moore et al., 2013) and metabolic functions of phytoplankton and consequently the efficiency of the biological carbon pump (Boyd et al., 2007; 2010). The primary factors that limit carbon fixation during phytoplankton photosynthesis in the Southern Ocean are the availability of light (Kirk, 1994) and several essential trace metals (Sunda, 1989; Lindsey and Scott, 2010; Browning et al., 2021), particularly iron, which is a crucial co-factor for the functioning of photosynthetic proteins (Raven, 1990; Raven et al., 1999; Strzepek and Harrison, 2004). In addition, iron is needed for nitrate reductase, which is responsible for the reduction of nitrate to nitrite (de Baar et al., 2005; Sunda, 1989), and is also required for the synthesis of chlorophyll and the quenching of reactive oxygen species (Sunda and Huntsman, 1995). Thus, independent of adequate amounts of macronutrient concentrations in surface waters, any limitation on the bioavailability of iron will potentially decrease the efficiency of these processes (Martin and Fitzwater, 1988), affecting nutrient drawdown, photosynthesis, primary productivity, biomass accumulation, and community composition of surface phytoplankton in the Southern Ocean (de Baar et al., 1990; Geider and La Roche, 1994; Martin et al., 1991; Martin and Fitzwater, 1988). Furthermore, any light limitation will exacerbate iron limitation due to the increase in iron demand under low light conditions (Strzepek et al., 2012), thus driving the frequent occurrence of iron-light co-limitation conditions in the Southern Ocean (Moore et al., 2013; Tagliabue et al., 2014; Ryan-Keogh et al., 2017a).

Although the Southern Ocean is typically considered an "iron-limited" region, iron availability or limitation is not uniform, and instead varies spatially and temporally. For instance, iron limitation is commonly associated with the pelagic waters of the Southern Ocean (Mitchell et al., 1991), where summer dissolved iron (dFe) concentrations in surface waters are typically <0.5 nM (Sedwick et al., 1999; Coale et al., 1999; Vink and Measures, 2001); however, there are a number of regional exceptions. These include regions with an external iron source such as sea-ice and iceberg meltwaters (Lannuzel et al., 2008; Boyd and Ellwood, 2010; Smith et al., 2010; Boyd et al., 2012), hydrothermal vents (Klunder et al., 2011; Tagliabue et al., 2017; Ardyna et al., 2019), atmospheric dust (Martin and Fitzwater, 1988; Mahowald et al., 2005), continental margins input (Sedwick et al., 2008; Bowie et al., 2009) and island wake inputs (Pollard et al., 2007; Blain et al., 2008). Internal processes such as remineralization (Tagliabue et al., 2017), resupply through deep winter mixing (Tagliabue et al., 2014), cross-frontal mixing (Lutjeharms et al., 1985; Moore and Abbott, 2002) and storm-driven entrainment

https://doi.org/10.5194/bg-2022-245
Preprint. Discussion started: 6 January 2023
© Author(s) 2023. CC BY 4.0 License.

(Nicholson et al., 2019) can also provide iron to surface waters in support of phytoplankton production. Most of these sources vary seasonally; for example, in winter, iron is not generally considered limiting as deep winter mixing entrains a seasonal resupply of iron (Tagliabue et al., 2014; Mtshali et al., 2019). Instead, due to the deep seasonal mixed layers, ice cover and low sun angles, the availability of photosynthetically active radiation (PAR) can be suboptimal and considered the dominant factor limiting phytoplankton production in winter. In spring, phytoplankton blooms are initiated when there is sufficient light, driven by a shoaling of the mixed layer as well as retreating sea-ice (Taylor et al., 2013) to support phytoplankton growth under nutrient replete conditions (Swart et al., 2015). Blooms typically subside when nutrients such as iron are depleted in late summer or early autumn (Tagliabue et al., 2014; Soppa et al., 2016). Grazing (Lancelot et al., 1993; Moreau et al., 2020; Kauko et al., 2021), bacteria and viruses (Biggs et al., 2021) may also accelerate the blooms' demise. Iron supply mechanisms during the bloom, such as advection from continental margins (Sedwick et al., 2008; Bowie et al., 2009), remineralization (Tagliabue et al., 2017) and storm-driven entrainment (Swart et al., 2015; Nicholson et al., 2019) may sustain phytoplankton growth for an extended duration. However, it is not clear how applicable these resupply processes are to the Southern Ocean as a whole, and where and when each of these dominate.

In general, experiments that investigate the degree of iron limitation by testing the impact of iron addition on metabolic functions of phytoplankton have largely focussed on summer conditions in the open Southern Ocean. There is thus minimal information on the impact of iron addition in the Sea-Ice Zone (SIZ) in autumn, when iron concentrations are expected to be low (Tagliabue et al., 2014). One exception was a study by Van Oijen et al. (2004), where a single iron-light perturbation experiment examined carbon uptake in the marginal ice zone in autumn, but no conclusions were made on the driving factors of enhanced uptake. To address this knowledge gap, we undertook a number of iron addition experiments using active chlorophyll-a (Chl-a) fluorescence in the SIZ off Dronning Maud Land (DML) in autumn (March). Active Chl-a fluorescence is a key indicator of the photophysiological state of phytoplankton (Hughes et al., 2018) and provides a powerful tool for evaluating the photophysiological response of phytoplankton to iron addition, i.e. by measuring the photosynthetic efficiency, F_v/F_m, and the absorption cross-section of photosystem II, σ_{PSII} (Geider, 1993; Geider and La Roche, 1994; Kolber et al., 1988; 1994). Any photophysiological response measured through active Chl-a fluorescence can, however, be due to both changes in cellular structure, i.e., a response seen on short timescales (milliseconds to femtoseconds), and changes in community structure, i.e., a response seen on longer time scales (usually >24 hrs). Since different phytoplankton groups tend to have different photophysiological signatures (Suggett et al., 2009), any measured response in photophysiology over longer time periods (>24 hrs)

https://doi.org/10.5194/bg-2022-245
Preprint. Discussion started: 6 January 2023
© Author(s) 2023. CC BY 4.0 License.

is difficult to interpret as it reflects both the cellular and community adjustments. This makes it difficult to disentangle the physiological response of phytoplankton to iron addition in manipulation incubation experiments from community structure adjustments (Suggett et al., 2009).

A number of iron addition incubation experiments previously conducted in the Southern Ocean (de Baar et al., 1990; Hinz et al., 2012; Ryan-Keogh et al., 2018; Viljoen et al., 2018) were run for long time periods (>96 hrs), and showed evidence of substantial changes in community structure, which are likely to influence the photophysiological signal and consequently the interpretation of iron limitation (Ryan-Keogh et al., 2013; Suggett et al., 2009). In this paper, we opted instead for short-term (24 hr) incubation experiments to isolate changes in photophysiology. This is in line with a study by Ryan-Keogh (2014), which tested whether 24 hrs was sufficient to allow a measurable photophysiological response in Southern Ocean phytoplankton, where low temperatures may control uptake kinetics. The study compared the photophysiology between incubations running for 24 and 48 hrs in summer and found that the stations were iron-limited (i.e. the differences between unamended control and iron addition incubations were significant). However, no significant differences were observed in photophysiology following iron addition when comparing the incubations of 24 vs 48 hrs, supporting the robustness of a representative response in photophysiology within 24 hrs. During this timeframe, the community structure is not expected to change, nor would we expect to see any adjustments in biomass or nutrient drawdown (Browning et al., 2014a; Ryan-Keogh et al., 2013; 2017a). As such, this study provides a unique investigation of the short-term photophysiological response of phytoplankton to iron addition in the SIZ in autumn, a season where iron limitation may be expected and a season and region that is under sampled. The experiments test the hypothesis that phytoplankton in the SIZ off DML experience iron limitation during post-bloom conditions in autumn.

2 Materials and methods

The focus of this study is on five short-term (24 hr) incubation experiments performed in March during the Southern Ocean Ecosystem Cruise (cruise number DML2019702) between 28th February and 10th April in 2019, on-board the Norwegian RV *Kronprins Haakon* in the SIZ of the Kong Håkon VII Hav off the Dronning Maud Land coast, as well as areas surrounding the Astrid Ridge (Fig. 1a). Ancillary data from surface water samples provide information on the regional conditions surrounding the five incubation experiments at the time of the cruise.

https://doi.org/10.5194/bg-2022-245
Preprint. Discussion started: 6 January 2023
© Author(s) 2023. CC BY 4.0 License.

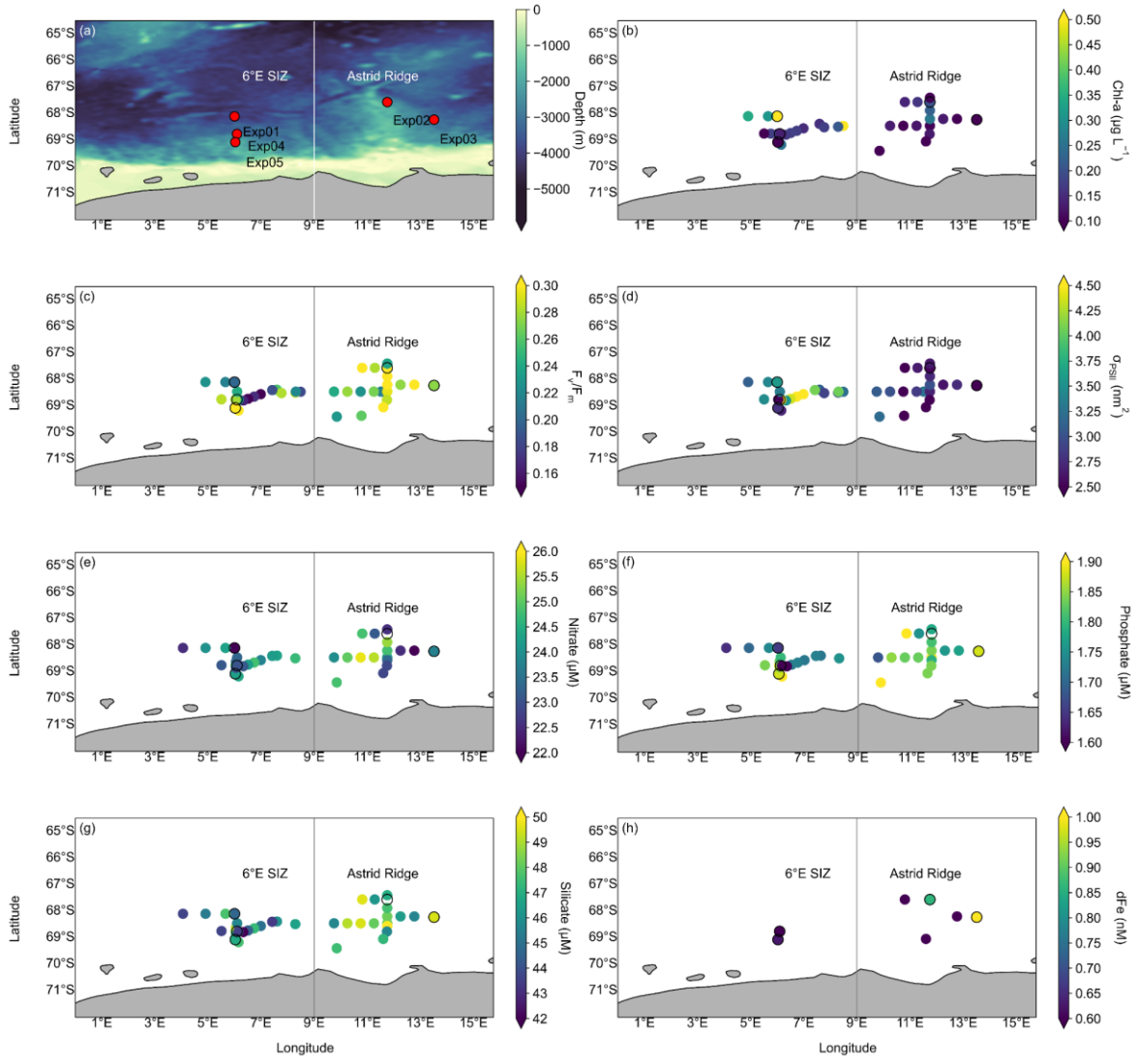

Figure 1. Initial conditions of the study region. Plots of (a) the overlaid bathymetry of the study region where the 6°E SIZ and Astrid Ridge region are indicated, along with the sampling locations for the incubations; and the associated mean initial parameters for (b) Chl-a concentrations (µg L^{-1}), (c) F_v/F_m, (d) σ_{PSII} (nm^2), (e) Nitrate (µM), (f) Phosphate (µM), (g) Silicate (µM) and (h) dFe concentration (nM). Underway measurements are shown with surface CTD data for (b-g) along with the initial incubation values. Plot (h) shows the dFe concentrations which were sampled at all the Go-Flo stations. All data for incubation stations are given in Table 1, and incubation stations are indicated by black circle outline in (b-h).

https://doi.org/10.5194/bg-2022-245
Preprint. Discussion started: 6 January 2023
© Author(s) 2023. CC BY 4.0 License.

Table 1. Sampling location information for the incubation stations with the associated CTD-Rosette water column station numbers from the cruise (CTD cast identifier) and mean initial parameters for the photophysiology (F_v/F_m and σ_{PSII}), as well as the associated ancillary data. Cumulative photon dose and euphotic depth were calculated as defined in Materials and methods. Mixed Layer Depth (MLD) was obtained from Kauko et al. (2021). Sea surface temperatures were obtained from the CTD sensor and were averaged for depths 15 to 30 m. Community structure was taken from a combination of microscopy and CHEMTAX data from Kauko et al. (2022a; 2022b). "n.d" indicates that no data was available and "±" precedes standard deviation.

	Experiment				
	Exp01	**Exp02**	**Exp03**	**Exp04**	**Exp05**
CTD identifier	CTD53	CTD70	CTD83	CTD97	CTD105
Initiation Date	12/03/2019	17/03/2019	19/03/2019	24/03/2019	26/03/2019
Initiation Time (UTC)	08h18	08h33	19h34	23h26	09h12
Latitude (°S)	68.10	67.56	68.23	68.76	69.07
Longitude (°E)	6.00	11.75	13.51	6.09	6.03
Sunrise (UTC)	05h02	04h57	04h57	05h45	05h53
Sunset (UTC)	18h27	17h45	17h30	17h38	17h30
Cumulative photon dose (mol photons m^{-2} d^{-1})	124	156	160	93	92
MLD (m)	38	27	36	28	30
Euphotic depth (m)	31	50	n.d	n.d	53
Mean PAR in the mixed layer (µmol photons m^{-2} s^{-1})	16.65	109.86	n.d	n.d	134.08
Sea Surface Temperature (°C)	-0.33	-1.16	-1.76	-1.71	-1.86

https://doi.org/10.5194/bg-2022-245
Preprint. Discussion started: 6 January 2023
© Author(s) 2023. CC BY 4.0 License.

F_v/F_m	0.20±0.01	0.34±0.02	0.35±0.01	0.32±0.03	0.28±0.01
σ_{PSII} (nm^2)	3.99±0.37	2.72±0.08	2.45±0.12	3.13±0.54	2.92±0.54
Chl-a (µg L^{-1})	0.73	0.23	0.02	0.18	0.14
Nitrate (µM)	22.5	26.2	25.5	25.8	25.7
Phosphate (µM)	1.67	1.71	1.69	1.72	1.75
Silicate (µM)	43	48	48	43	44
dFe (nM)	n.d	0.86±0.05	1.39±0.14	0.56±0.05	0.63±0.13
Community Structure	High diatom abundance, Flagellates, dinoflagellates	Pennate diatoms and centric diatoms	Pennate diatoms and centric diatoms	Flagellates	Flagellates

2.1 Underway and surface CTD seawater sampling and measurements

Underway seawater was obtained from the ship's clean seawater sampling system at ~4 m depth between incubation stations. Samples were collected for determining Chl-a concentration, macronutrient concentrations (nitrate, phosphate and silicate) and photophysiology (F_v/F_m and σ_{PSII}) (Kauko et al., 2020; 2021; 2022a; 2022b; Chierici and Fransson, 2020; Singh et al., 2022). Additionally, surface seawater samples were collected using a Seabird CTD (conductivity-temperature-depth) rosette sampler and similarly analysed for Chl-a, macronutrients and photophysiology in addition to phytoplankton community composition (Kauko et al., 2020; 2021; 2022a; 2022b; Chierici and Fransson, 2020; Singh et al., 2022). Sample processing and analysis are further detailed in section 2.4 for phytoplankton photosynthetic photophysiology and sections 2.5 - 2.10 for ancillary data. In addition, initial in situ conditions for the incubation experiments from CTD surface samples are detailed below in section 2.3 (Incubation set-up and sub-sampling).

https://doi.org/10.5194/bg-2022-245
Preprint. Discussion started: 6 January 2023
© Author(s) 2023. CC BY 4.0 License.

2.2. Surface seawater sampling for incubation experiments

A trace metal clean, Teflon-lined, external closure 8 L Go-Flo bottle (General Oceanics), was deployed on an aramid rope (VGP industri), using a dedicated winch and Teflon coated messenger to ~20 - 30 m depth for surface incubation seawater (i.e. for experimental stations Exp02, Exp03, Exp04 and Exp05; see Fig. 1a and Table 1 for locations). Seawater samples for experimental station Exp01 were collected at 20 m depth using a Watson Marlow Varmeca (MG0723) peristaltic pump connected to PTFE tubing with a 10 mm inner diameter at a flow rate of 1.6 L min^{-1}. All sampling tubing (peristaltic and PTFE) and 1 L Polycarbonate bottles (ThermoFisher Scientific Nalgene) were acid-washed following GEOTRACES protocols (Cutter et al., 2017). The seawater was pumped in a custom-made HEPA air-filtered Class-100 trace metal clean 'plastic bubble', that consisted of a clean, steady laminar flow hood (AirClean-600 PCR Workstation), under strict trace metal clean conditions. At each of the five experimental stations, seven 1 L polycarbonate bottles were used to collect the incubation seawater. These seven 1 L polycarbonate bottles were filled unscreened to represent 1 x the initial sample (hereafter 'initial'), 3 x the unamended control samples (hereafter 'Control'), and 3 x iron addition samples (hereafter 'Fe'), which were spiked with 2.0 nM iron (III) chloride ($FeCl_3$ TraceCERT®; Sigma Aldrich) prepared in 2‰ HCl (30% suprapur HCl; Merck). The bottle caps of the Control and Fe samples were sealed with Parafilm™, and the bottles were double-bagged in clear polyethylene bags (ZipLoc™) to avoid sample contamination. All incubation bottle filling, spiking and sub-sampling were performed under a clean, laminar flow hood (AirClean-600 PCR Workstation), inside a makeshift HEPA air-filtered Class-100 trace metal clean bubble on-board, under strict trace metal clean conditions.

2.3. Incubation set-up and sub-sampling

The incubation bottles were placed inside an on-deck incubator under natural sunlight, with flowing seawater, which fluctuated with the ocean temperature, passing through the incubator to mimic in situ seawater temperatures. The seawater temperature was measured at the ship's intake by a thermosalinograph. Light levels inside the polycarbonate bottles were measured using a handheld 4π PAR sensor (Biosphere QSL 2100, Biospherical Instruments Inc.) with the Logger 2100 software. A green mesh was used to filter out a fraction of the PAR on Exp01, with the PAR measured inside the incubator bottle being 37% of sea surface PAR, whilst the remaining experiments had no filters on the incubators, and the average PAR corresponded to 43% PAR at the sea surface inside the incubator bottle. After each 24 hr period, the experiment was terminated and the incubation bottles removed from the incubator and sub-sampled under the clean, laminar flow hood (AirClean-600 PCR Workstation), inside the makeshift HEPA air-filtered Class-100 trace metal clean plastic bubble on-

https://doi.org/10.5194/bg-2022-245
Preprint. Discussion started: 6 January 2023
© Author(s) 2023. CC BY 4.0 License.

board as described above in section 2.2. All incubation bottles were sub-sampled for photophysiological parameters using active Chl-a fluorescence measured through Fast Repetition Rate fluorometry (FRRf) (see section 2.4), Chl-a concentration (see section 2.5) and macronutrients (see section 2.6). A complete list of sampling locations, initial parameters for the photophysiology and ancillary data, as well as other relevant information (cumulative photon dose, MLD, euphotic depth and sea surface temperatures) is provided in Table 1.

2.4. Phytoplankton photosynthetic photophysiology (FRRf)

Active Chl-a fluorescence was measured with a FastOcean™ FRRf incorporating a FastAct™ laboratory system (Chelsea Technology Group), operated with the single-turnover protocol set with a flash saturation sequence (100 x 1 µs flashlets with a 2 µs interval) and a relaxation sequence (25 x 1 µs with an interval of 84 µs). The power of the excitation LED (λ_{450nm}) was adjusted between samples to saturate the observed transients following manufacturer specifications. All samples were dark acclimated for ~30 min under in situ temperatures prior to measurement of the photophysiological (fluorescence) parameters (F_v/F_m and σ_{PSII}) (Roháček, 2002) and were each blank corrected using carefully prepared 0.2 µm filtrates (Cullen and Davis, 2003). The FRRf measurements were recorded with the FastPro8 software (v1.0.55), and post-processing analysis was done in Python 3.7, using the customized package Phytoplankton Photophysiology Utilities (Ryan-Keogh and Robinson, 2021). The fluorescence response data were fitted to the saturation phase of the biophysical model of Kolber et al. (1998), with a constant connectivity coefficient ρ, of 0.3 (Suggett et al., 2001) to derive F_o, F_m and F_v/F_m. The sample means and the standard deviation (SD) were calculated for F_v/F_m and σ_{PSII} from each set of triplicate samples. Statistical t-tests were performed to compare the mean F_v/F_m and σ_{PSII} values between the Control and Fe samples. Results of the t-tests are reported as statistically significant at the 95% confidence level ($p<0.05$).

2.5. Chl-a

A volume of 500 – 1000 mL of seawater was filtered for Chl-a extraction onto GF/F filters (nominal pore size 0.7 µm; GE Healthcare) under low vacuum pressure (ca -30 kPa). Chl-a was extracted with 100% methanol at 4°C in the dark for 24 hrs (Holm-Hansen and Riemann, 1978) and was subsequently measured on-board, using a Turner 10-AU Fluorometer (Turner Designs) which was calibrated prior to the cruise using a standard calibration curve from raw chlorophyll (Sigma C6144).

https://doi.org/10.5194/bg-2022-245
Preprint. Discussion started: 6 January 2023
© Author(s) 2023. CC BY 4.0 License.

2.6. Macronutrients

The seawater samples for macronutrient analysis (nitrate, phosphate and silicate) were collected in 50 mL Falcon tubes and preserved with 250 µL of chloroform. The samples were kept cold and in the dark until post-cruise analysis at the Institute of Marine Research, Bergen, Norway, using standard methods (Grasshoff et al., 2009) and a Flow Solution IV analyser from O.I. Analytical. The analyser was calibrated using reference seawater from Ocean Scientific International Ltd. The detection limits were 0.5 µM for nitrate, 0.06 µM phosphate and 0.7 µM for silicate.

2.7. Dissolved Fe (dFe)

Seawater samples for dFe measurements were collected from the clean Go-Flo bottles (5L General Oceanics), at seven stations in the study region (unfortunately, a dFe sample is not available for experimental station Exp01), into acid washed 125 ml low-density polyethylene (LDPE, Nalgene, ThermoScientific) sampling bottles. The LDPE bottles were acid cleaned according to the GEOTRACES protocols (Cutter et al., 2017) prior to the cruise. The dFe samples were filtered through sequential Sartorius capsule filters (0.45 and 0.2 µm pore size filtration) using acid-washed Tygon tubes inside the trace metal clean plastic bubble. During filtration, an additional HEPA air-filter cartridge (HEPA-CAP/HEPA VENT, 75 mm, Whatman) was connected to the pressure relief valve of the Go-Flo bottles to ensure that the air in contact with the sample during the filtration was clean. All samples were acidified to pH < 2 with 600 µL of ~3 M double quartz distilled ultrapure HNO_3 (VWR, AnalaR NORMAPUR® analytical reagent), double-bagged and stored at room temperature (> 2 years) until analysis at Stellenbosch University (TracEx, South Africa) as described in Samanta et al. (2021) using online pre-concentration methods. Although the samples were stored for more than two years before analysis, the dFe concentration is unlikely to be affected. The long-term analyses (2017-2021) of GEOTRACES and Certified reference standards, which yielded consistent dFe concentrations support this conclusion (Samanta et al., 2021). All samples were measured in duplicate. The detection limit of Fe was 0.08 nM.

2.8. Satellite Chlorophyll Data

Ocean colour data (8 days, 4 km) were obtained from the ocean colour climate change initiation (OC-CCI) (Sathyendranath et al., 2019). In order to reduce missing data, satellite-derived Chl-a values were first re-gridded to a 4 km regular grid by averaging all data points within the new pixel dimensions. Gaps in the data were filled by applying a linear interpolation scheme as defined in Racault et al. (2014). The data were

https://doi.org/10.5194/bg-2022-245
Preprint. Discussion started: 6 January 2023
© Author(s) 2023. CC BY 4.0 License.

smoothed by applying a moving average filter of the previous and next time step (for more details on this method see Salgado-Hernanz et al. (2019)). Two boxes were defined for the respective regions of this study and averaged to get the annual cycle of Chl-a concentration: 6°E SIZ (62 - 72°S; 0 - 9°E) and Astrid Ridge (62 - 72°S; 9 - 16°E) (Fig. 2).

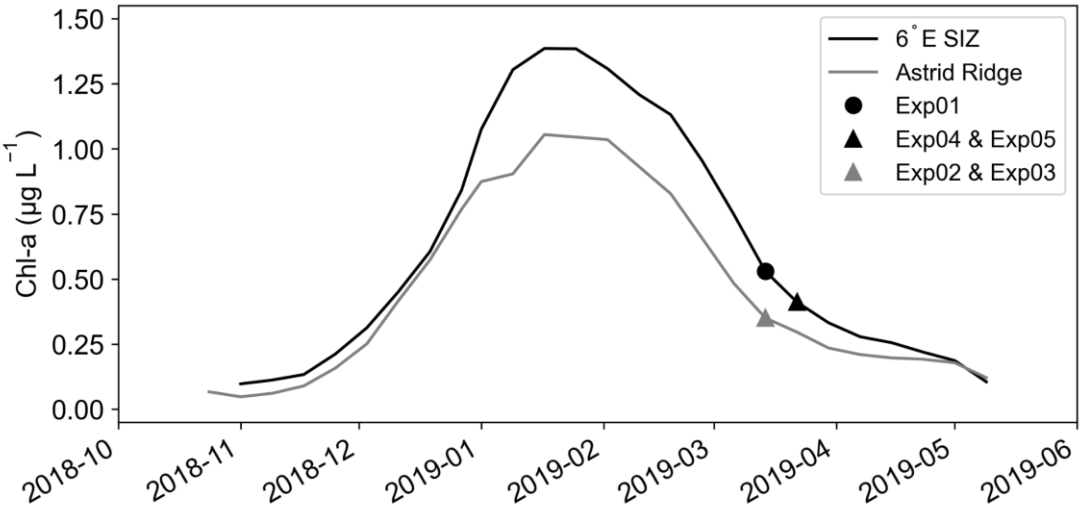

Figure 2. Satellite chlorophyll-a (Chl-a; µg L^{-1}) data from OC-CCI from 01/10/2018 to 01/06/2019. The 6°E SIZ (62 - 72°S; 0 - 9°E) and Astrid Ridge (62 - 72°S; 9 - 16°E) were created from spatial means as indicated in the methods. The dates of the experimental set-ups are included for each region.

2.9. PAR sensor data

The cumulative photon dose for each experiment (mol photons m^{-2} d^{-1}) was calculated as the cumulative sum of the surface PAR measured by a Biospherical Licor Chelsea PAR sensor on the ship's mast, starting from the time of experimental commencement, until experiment termination. Values were adjusted by ~43% to account for shading within the incubator in accordance with the measured sea surface PAR inside the incubator.

2.10. Bathymetry data, stratification, the Mixed Layer Depth (MLD) and euphotic depth

The ETOPO1 bathymetry data for the study region was extracted from ("*ETOPO1, Global 1 Arc-minute Ocean Depth and Land Elevation From the US National Geophysical Data Center (NGDC)*," 2011). The degree of stratification was obtained from the Brunt-Väisälä frequency (N^{2-}; s^{-1}) (Millard et al., 1990), which was calculated using the seawater temperature, salinity and potential density (σ) at each experimental station. The

https://doi.org/10.5194/bg-2022-245
Preprint. Discussion started: 6 January 2023
© Author(s) 2023. CC BY 4.0 License.

MLD for each experimental station was obtained from Kauko et al. (2021) and the respective euphotic depth was determined as the depth at which PAR is 1% of surface PAR, based on Kirk (1994).

3 Results

In accordance with published work from this cruise (Kauko et al., 2021), two distinct regions were identified in the DML SIZ. Both regions were visited in post-bloom conditions (Kauko et al., 2021), but differed in the peak Chl-a concentrations, i.e. in the bloom amplitude (Fig. 2). The first was a region in shallower bathymetry (~2556±724 m depth, 11°E - 14°E, 67°S - 69°S) around Astrid Ridge (Fig. 1a). Two short-term iron addition incubation experiments, Exp02 and Exp03, were conducted in this region, north and east of Astrid Ridge, respectively (Table 1; Fig. 1a). The second region in deeper bathymetry (~3042±1129 m depth, 5°E - 7°E, 67°S - 70°S) was located on a 6°E transect to the west of the Astrid Ridge in the open-ocean SIZ (6°E SIZ) (Fig. 1a), where the experimental station Exp01 was conducted. Despite being occupied in post-bloom conditions from a seasonal perspective (Fig. 2), Exp01 was, nonetheless, considered to represent autumn bloom conditions (albeit in decline) with high Chl-a concentrations (0.73 µg L^{-1}) (Kauko et al., 2021). Experimental stations Exp04 and Exp05 were sampled two weeks after Exp01, which was after the seasonal bloom (Chl-a = 0.18 µg L^{-1} and 0.14 µg L^{-1}, respectively) within the same 6°E SIZ region. We note that the starting time of each incubation was not synchronized (Table 1) and may lead to issues in interpreting photophysiological responses due to diurnal variation (Schuback et al., 2016). However, we found no distinct diurnal differences in both F_v/F_m and σ_{PSII} across the 6°E SIZ and Astrid Ridge regions (Fig. A3), with both parameters showing very little variability between local sunrise and sunset.

Here, we first characterise the general conditions in these two regions and then focus specifically on the five experimental stations. Chl-a concentrations were lower around Astrid Ridge, ranging from 0.03 µg L^{-1} to 0.26 µg L^{-1} (mean 0.12±0.07 µg L^{-1}; n=16), whilst concentrations between 0.07 µg L^{-1} and 1.02 µg L^{-1} (mean 0.25±0.24 µg L^{-1}; n=18) were observed in the 6°E region of the SIZ (Fig. 1b; Table B1). The mean values of F_v/F_m (Fig. 1c) were higher at Astrid Ridge (0.28±0.04) compared to the 6°E SIZ (0.24±0.06). The 6°E SIZ showed a much larger range in F_v/F_m with a minimum of 0.07 and a maximum of 0.34, whilst a narrower range in F_v/F_m, with a higher minimum in particular, was seen around Astrid Ridge (0.21 to 0.36). The σ_{PSII} (Fig. 1d) was typically higher in the 6°E SIZ region, ranging from 2.48 to 5.63 nm^2 (mean 3.41±0.71 nm^2) and lower around the Astrid Ridge, 1.93 to 3.56 nm^2 (mean 2.66±0.37 nm^2).

https://doi.org/10.5194/bg-2022-245
Preprint. Discussion started: 6 January 2023
© Author(s) 2023. CC BY 4.0 License.

Surface nitrate concentrations showed some spatial variability, but the mean values were similar for the 6°E SIZ (mean 23.8±0.8 µM) and Astrid Ridge (mean 24.0±1.2 µM) (Fig. 1e). This similarity between the regions was also observed for phosphate concentrations, which ranged from 1.57 to 1.96 µM in the 6°E SIZ (mean 1.75±0.10 µM), and from 1.68 to 1.92 µM at Astrid Ridge (mean 1.82±0.06 µM) (Fig. 1f). Silicate concentrations showed a higher mean (48±1 µM) and less variability around Astrid Ridge with concentrations ranging from 46 to 52 µM, compared to a lower mean (46±2 µM) and larger range (41 to 49 µM) observed in the 6°E SIZ (Fig. 1g). Despite the limited number of dFe measurements, a wide range of surface concentrations (Fig. 1h) were evident around Astrid Ridge with concentrations as low as 0.27 nM and as high as 1.39 nM (mean 0.64±0.49 nM). Mean dFe concentrations in the 6°E SIZ were slightly lower (0.59±0.05 nM) compared to Astrid Ridge and varied over a narrow range between 0.56 to 0.63 nM. Furthermore, the mean PAR in the mixed layer for the 6°E SIZ was lower (29.71 µmol photons m^{-2} s^{-1}) in comparison to the Astrid Ridge (59.37 µmol photons m^{-2} s^{-1}).

In the following, we focus particularly on the upper ocean conditions at stations where incubation experiments were conducted (Table 1). Initial conditions in surface Chl-a ranged from high concentrations at the bloom station Exp01 (0.73 µg L^{-1}) dropping to as low as 0.02 µg L^{-1} at Exp03 in the Astrid Ridge. Similar to the general oceanographic conditions, both nitrate and phosphate showed very little variability between experiments, whereas silicate concentrations were slightly lower for all three stations in the 6°E SIZ (43 – 44 µM) in comparison to the Astrid Ridge (48 µM). Unfortunately, the initial dFe concentration at the bloom station Exp01 is not available, however, dFe concentrations tended to be lower at the remaining stations (Exp04 and Exp05) in the 6°E SIZ (0.56 – 0.63 nM) compared to the Astrid Ridge (0.86 – 1.39 nM) (Table 1). The cumulative photon dose over 24 hrs (Table 1; Fig. A1) were substantially different, as Exp01, Exp02 and Exp03 (124 - 160 mol photons m^{-2} d^{-1}) had much higher doses compared to Exp04 and Exp05 (92 - 93 mol photons m^{-2} d^{-1}). The MLD at all experimental stations showed little variability (Kauko et al., 2020; 2021; Table 1; Fig. A2) ranging between 27 and 38 m (mean 31±5 m). The degree of stratification, however, ranged substantially being particularly stratified at the bloom station (Exp01), with a high degree of variability in the Brunt-Väisälä frequency (N^2) at the MLD, and comparatively weakly stratified at Exp05, with very little variability in the profile of N^2 (Fig. A2). The euphotic depth ranged from 31 to 53 m at the three stations where CTD profiles were collected during daylight hours (Table 1). Since the euphotic depth was typically deeper than the MLD, these stations may unlikely be light-limited. However, mean PAR in the mixed layer had a broad range from 16.65 µmol photons m^{-2} s^{-1} (Exp01) to 134.08 µmol photons m^{-2} s^{-1} (Exp05), that likely reflects the degree of cloudiness (since time of day was similar), thus preventing us from making any concrete conclusions on light

https://doi.org/10.5194/bg-2022-245
Preprint. Discussion started: 6 January 2023
© Author(s) 2023. CC BY 4.0 License.

limitation. Although still in the negative, surface temperatures were warmer at the bloom station Exp01 (-0.33°C) and cooler at the remaining stations (-1.16 to -1.86°C) (Table 1).

Given the variability described above, it is anticipated that initial conditions of F_v/F_m and σ_{PSII} would vary between incubation stations (Table 1; Fig. 3). F_v/F_m was lower in the 6°E SIZ (mean 0.27±0.01) compared to Astrid Ridge (mean 0.35±0.01) and was particularly low at the bloom station Exp01 (0.20±0.01). The opposite was true for σ_{PSII} with initial conditions being higher in the 6°E SIZ (mean 3.35±0.28 nm^2) and the highest σ_{PSII} at Exp01 (3.99±0.37 nm^2) with the lowest σ_{PSII} at the Astrid Ridge (mean 2.59±0.05 nm^2). The differences in these initial conditions, i.e. seasonal timing and bloom amplitude, dFe surface concentrations, as well as F_v/F_m and σ_{PSII}, indicate that some variability in the photophysiological response to iron addition could be anticipated. Nonetheless, despite these initial differences in conditions, very little variability was observed in the photophysiological response to iron addition (Fe) relative to the Controls (Fig. 3; Table 2). A statistical paired t-test between Fe and Control samples confirmed this, with no significant differences ($p>0.05$) in the photophysiology (F_v/F_m or σ_{PSII}) evident for any of the incubation experiments between treatments (Table 2). Similarly, no significant differences ($p>0.05$) were observed in either macronutrient or chlorophyll concentrations (Table 2) between the Fe and Control incubations.

https://doi.org/10.5194/bg-2022-245
Preprint. Discussion started: 6 January 2023
© Author(s) 2023. CC BY 4.0 License.

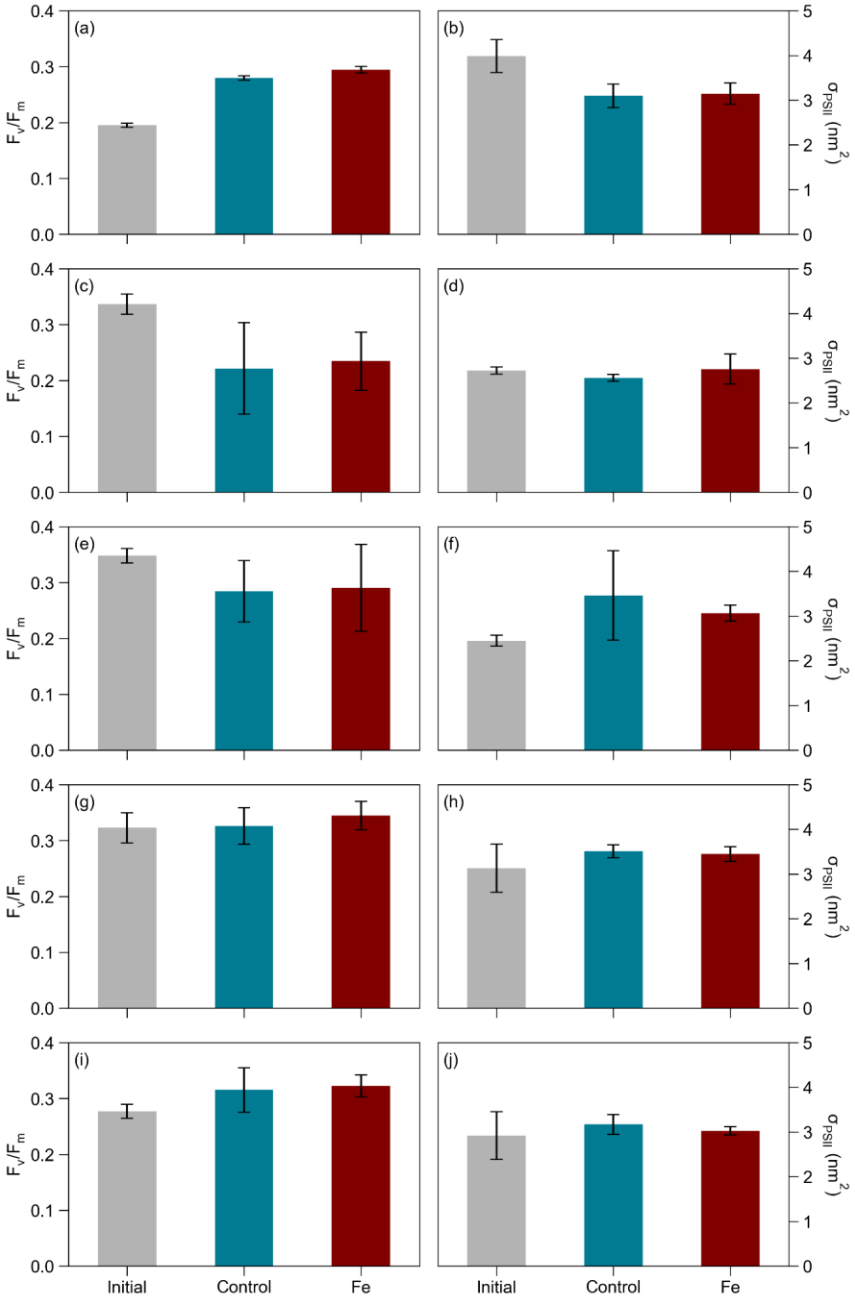

Figure 3. The mean F_v/F_m and mean σ_{PSII} (nm^2) from the initial, control and the Fe treatments, where error bars indicate standard deviations. (a,b) Exp01; (c,d) Exp02; (e,f) Exp03; (g,h) Exp04 and (i,j) Exp05.

https://doi.org/10.5194/bg-2022-245
Preprint. Discussion started: 6 January 2023
© Author(s) 2023. CC BY 4.0 License.

Table 2. Associated mean (± standard deviations) parameters of the Control and Fe samples measured post-incubation for F_v/F_m, σ_{PSII} (nm^2), Chl-a concentrations (µg L^{-1}) and the macronutrients nitrate, phosphate and silicate (µM). "n.d" indicates that no data was available.

Experiment	F_v/F_m		σ_{PSII}		Chl-a		Nitrate		Phosphate		Silicate	
	Control	Fe	Control	Fe	Control	Fe	Control	Fe	Control	Fe	Control	Fe
Exp01	0.28±0.01	0.29±0.01	3.10±0.26	3.15±0.24	n.d	0.97±0.11	22.9±0.2	23.0±0.1	1.63±0.02	1.68±0.04	42±0	42±1
Exp02	0.22±0.08	0.23±0.05	2.56±0.07	2.76±0.34	0.19±0.02	0.15±0.02	26.4±0.2	27.8±0.6	1.66±0.02	1.69±0.01	48±0	47±1
Exp03	0.28±0.06	0.29±0.08	3.46±0.90	3.07±0.18	0.06±0.02	0.05±0.01	25.9±0.1	25.7±0.6	1.70±0.00	1.69±0.01	47±0	47±0
Exp04	0.33±0.03	0.34±0.03	3.51±0.15	3.45±0.16	0.18±0.02	0.17±0.01	26.0±0.4	25.7±0.6	1.74±0.01	1.73±0.01	44±1	44±0
Exp05	0.32±0.04	0.32±0.02	3.17±0.22	3.02±0.09	0.15±0.00	0.13±0.01	26.4±0.4	26.1±0.3	1.76±0.01	1.74±0.01	45±0	46±0

https://doi.org/10.5194/bg-2022-245
Preprint. Discussion started: 6 January 2023
© Author(s) 2023. CC BY 4.0 License.

4 Discussion

Biological activity in the Southern Ocean is driven in part by high macronutrient availability, with primary production ultimately being constrained by the seasonal variability in light and the micronutrient iron (de Baar et al., 1990; Hauck et al., 2015; Martin et al., 1990). In addition to directly impacting photosynthesis, light also indirectly modulates the response of phytoplankton to iron availability (Boyd and Abraham, 2001; Moore et al., 2013), diminishing photosynthesis when iron concentrations are depleted (Hiscock et al., 2008; Moore et al., 2013; Ryan-Keogh et al., 2017b). The Southern Ocean phytoplankton are able to photophysiologically adapt to low light and low iron conditions by maximizing photosynthesis through an increase in the size (rather than the number) of their photosynthetic units, thus boosting access to available light without increasing their cellular iron demand (Raven, 1990; Strzepek et al., 2011; 2012; 2019; Sunda and Huntsman, 1997; Behrenfeld and Milligan, 2013). However, nitrate assimilation has a high iron (Milligan and Harrison, 2000; de Baar et al., 2005) and light (Lucas et al., 2007; Moore et al., 2007a; 2007b) demand, which drives the high-nutrient, low-chlorophyll (HNLC) conditions characteristic of the Southern Ocean (Price et al., 1994; Milligan and Harrison, 2000; Lucas et al., 2007; Cochlan, 2008; Moore et al., 2013). If primary production in the Southern Ocean were to be accurately quantified and constrained, a more detailed understanding of the regional and seasonal sensitivity of primary production to iron (and light) limitations are needed.

The majority of Southern Ocean incubation studies have shown that phytoplankton are iron-limited (de Baar et al., 1990; Viljoen et al., 2018; Ryan-Keogh et al., 2017a; 2018; Browning et al., 2014a; 2014b). However, no studies, to our knowledge, have been conducted in the SIZ during autumn. Furthermore, the majority of incubation studies were conducted as longer-term incubations (>96 hrs). The complexity induced by longer-term nutrient addition incubations are exacerbated by artifacts that cause an isolated system to be devoid of natural factors such as, nutrient resupply and grazing which differs between the initial and incubated samples, whilst retaining only a specific sampled section from the water column as representative of the entire system (Geider and La Roche, 1994). While short-term incubations, within 24 hrs, are also an isolated system devoid of these natural factors, the impact of these factors are reduced in the shorter incubation timeframe and increased by the longer incubation timeframe. Thus, short-term incubation studies provide a sufficient period for eliciting a measurable photophysiological response (Ryan-Keogh et al., 2017a), while at the same time minimising the possibilities of artifacts in the incubation, as evidenced by the absence of any significant differences in

https://doi.org/10.5194/bg-2022-245
Preprint. Discussion started: 6 January 2023
© Author(s) 2023. CC BY 4.0 License.

phytoplankton biomass or nutrient concentrations between the Control samples after incubation and the initial samples before incubation. Indeed, other studies in the Southern Ocean have also reported significant changes in F_v/F_m within 24 hrs following iron addition (Boyd and Abraham, 2001; Hinz et al., 2012; Browning et al., 2014a; 2014b; Ryan-Keogh et al., 2017a), suggesting that it is possible to determine rapid (<24 hrs) responses of photophysiology in iron-limited phytoplankton.

An annual time series of satellite-derived Chl-a averaged over the Astrid Ridge and 6°E SIZ region depicts the timing of the cruise relative to the seasonal cycle (Fig. 2) and clearly shows that both regional occupations were towards the end of the seasonal bloom. Therefore, it was anticipated that the region would be iron-limited and respond favourably to Fe addition. The study also covered a broad range of conditions when comparing the Astrid Ridge and 6°E SIZ regions (Fig. 1) i.e., shallower versus deeper bathymetry, lower versus higher biomass, lower versus higher dFe concentrations, lower versus higher F_v/F_m and higher versus lower σ_{PSII}. Similarly, phytoplankton communities between the two regions differed substantially (Kauko et al., 2022a; 2022b), where pennate and centric diatoms dominated in the Astrid Ridge region (Exp02 and Exp03), while the 6°E SIZ region consisted mostly of flagellates, with the exception of Exp01 that together with flagellates had a high abundance of diatoms. Despite contrasting conditions in physics (density, stratification, cumulative photon dose, mean PAR in the mixed layer), chemistry (nitrate, silicate and dFe) and biology (Chl-a, F_v/F_m, σ_{PSII} and community structure), none of the five iron incubation experiments displayed any significant differences between the Fe and the Controls for photophysiology, or for any of the ancillary parameters (Table 1 and Figs. A1 and A2). As such, iron was not considered limiting to photosynthesis at any of the autumn stations in the DML SIZ. This was unexpected and implies that despite the timing of the cruise occupation relative to the seasonal bloom termination, iron was unlikely the primary driver of the bloom's ending. Instead, grazing, bacteria, viral lysis, ice formation and/or wind mixing, anomalies in the easterly winds which could drive sea ice southwards, favouring upwelled iron-rich warmer deep water, and decreasing incident light may all be considered more important in curtailing the seasonal bloom in this particular region. Indeed, krill abundance estimates from Kauko et al. (2021) observed high concentrations of krill swarms around the 6°E transect, suggesting high levels of phytoplankton grazing.

These results also imply an internal short-term or continuous supply of dFe that prevent the bloom from exhausting a finite dFe reservoir that would otherwise be expected so late in the growing season from a water column characterised by a stratified freshwater lens. For example, dFe could be sourced from remineralisation, upwelled deep water, the continental margin, and/or shallow topography. Relatively high bacterial abundance

https://doi.org/10.5194/bg-2022-245
Preprint. Discussion started: 6 January 2023
© Author(s) 2023. CC BY 4.0 License.

was observed at both the Astrid Ridge (3.8 x 10^5 cells mL^{-1}) and in the Southern section of the bloom region along the 6°E transect (3.9 x 10^5 cells mL^{-1}), with lower abundance coinciding specifically with the bloom station Exp01 (2.6 x 10^5 cells mL^{-1}) (Kauko et al., 2021). A high bacterial abundance together with the seasonal timing of the cruise occupation (i.e. post-bloom peak in autumn), may support re-supply mechanisms such as remineralization as a potential source of iron (Tagliabue et al., 2017). This has been observed previously by Richert et al. (2019) during spring and summer in the Amundsen Sea, who suggested high bacterial abundance as a contributing factor to sustaining and promoting phytoplankton growth in autumn beyond the spring to summer bloom season. In addition, Kauko et al. (2021) utilised ~20 years of satellite-derived ocean colour data to suggest that the high bloom magnitude in this region was enhanced by flow patterns in the Weddell Gyre and tidal current interactions with seafloor topography enhancing primary productivity by natural fertilization.

5 Conclusions

The results from this study show that although in theory it is expected that parts of the Southern Ocean are iron-limited during autumn, it is not necessarily true for the Sea-Ice Zone region surrounding Astrid Ridge and along the 6°E transect, where high F_v/F_m and σ_{PSII}, i.e. efficient photophysiology was observed in situ, and where iron addition did not lead to more efficient photophysiology. The primary drivers of sustained iron supply to the region in support of phytoplankton growth late in the season are being potentially provided with both from below (i.e. vertical supply from shallow bathymetry interactions with currents) and from within (i.e. bacterial driven remineralisation), however, further examination of these sources and the type of iron being supplied is required to confirm the dominant resupply mechanism. It is recommended that future studies in this region help to bridge the knowledge gaps by studying the varying impacts of light in tandem with iron and other trace metals (e.g. manganese) which may instead be limiting during this time of the year, with an emphasis on short-term studies to understand the photophysiological response of phytoplankton in the absence of community induced responses.

https://doi.org/10.5194/bg-2022-245
Preprint. Discussion started: 6 January 2023
© Author(s) 2023. CC BY 4.0 License.

Biogeosciences Discussions
Open Access
EGU

Appendix A: Appendix figures

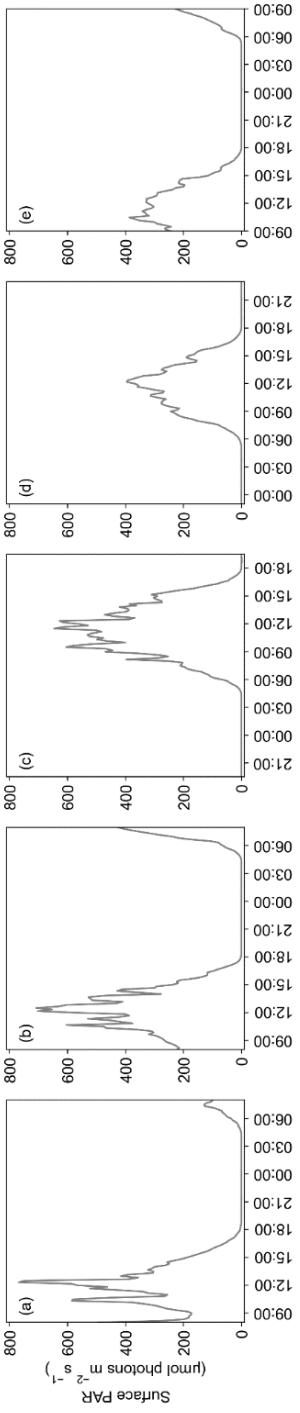

Figure A1. Surface PAR (µmol photons m^{-2} s^{-1}) at each experimental station (a) Exp01, (b) Exp02, (c) Exp03, (d) Exp04 and (e) Exp05. Data was plotted from the time of experimental set-up until the experiment was terminated 24 hrs later.

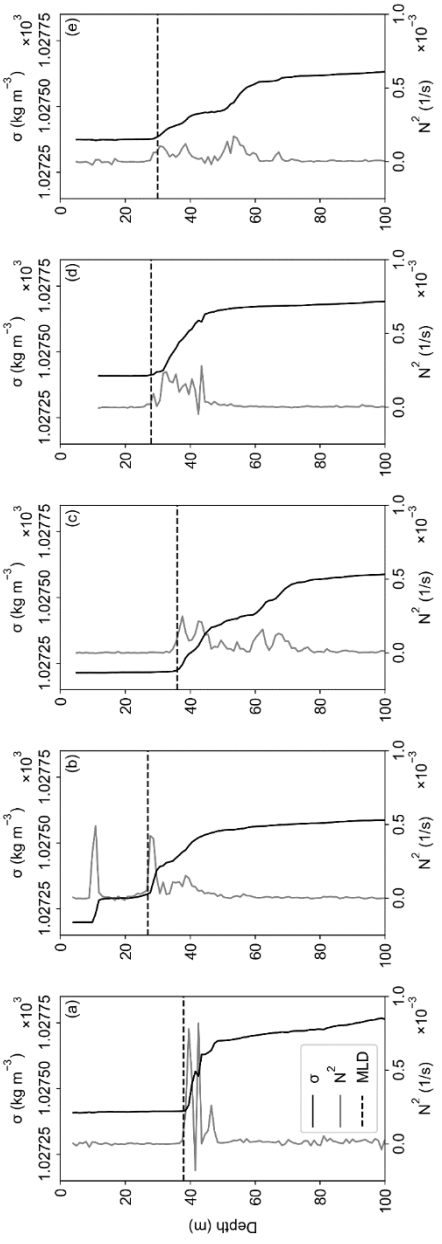

Figure A2. The depth profiles of density (σ; kg m^{-3}) and Brunt-Väisälä frequency (N^2) with the mixed layer depth (MLD; m) for experimental stations (a) Exp01, (b) Exp02, (c) Exp03, (d) Exp04 and (e) Exp05.

https://doi.org/10.5194/bg-2022-245
Preprint. Discussion started: 6 January 2023
© Author(s) 2023. CC BY 4.0 License.

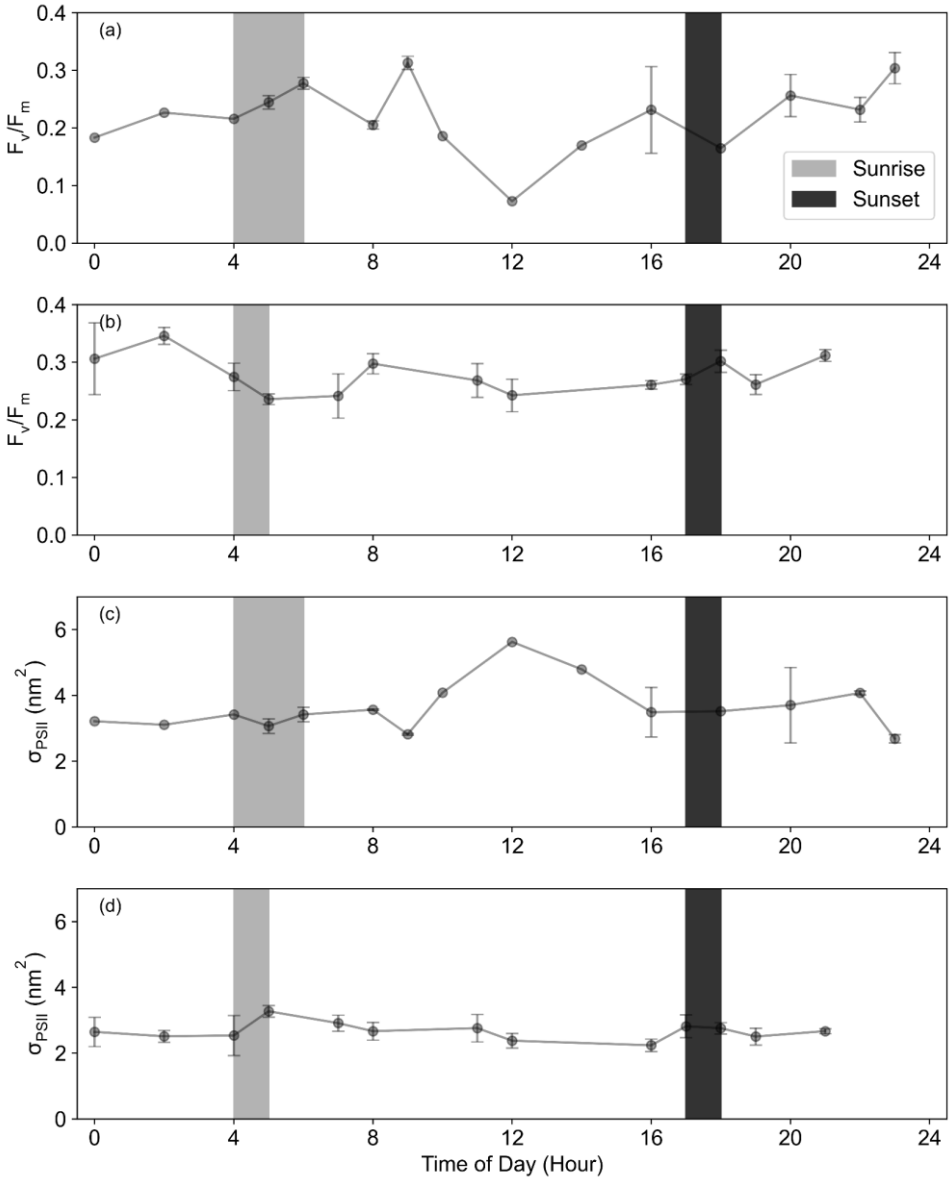

Figure A3. The diurnal cycle of (a,b) F_v/F_m for the (a) 6°E SIZ and (b) Astrid Ridge, and of (c,d) σ_{PSII} for the (c) 6°E SIZ and (d) Astrid Ridge, where the range of local sunrise and sunset times are indicated. Data were averaged together using the hour of the day, where error bars indicate standard deviation.

https://doi.org/10.5194/bg-2022-245
Preprint. Discussion started: 6 January 2023
© Author(s) 2023. CC BY 4.0 License.

Appendix B: Appendix tables

Table B1. Associated numbers (n), minimum, maximum and mean (± standard deviations) parameters for the 6°E SIZ and the Astrid Ridge for Chl-a concentrations (µg L^{-1}), F_v/F_m, σ_{PSII} (nm^2), macronutrients nitrate, phosphate and silicate (µM) and the dFe concentrations (nM).

		Chl-a	F_v/F_m	σ_{PSII}	Nitrate	Phosphate	Silicate	dFe
6°E SIZ	**min**	0.07	0.07	2.48	21.8	1.57	41	0.57
	max	1.02	0.34	5.63	24.8	1.96	49	0.63
	mean±SD	0.25±0.24	0.24±0.06	3.41±0.71	23.8±0.8	1.75±0.10	45±2	0.59±0.05
	n	18	33	33	21	21	21	2
Astrid Ridge	**min**	0.03	0.21	1.93	21.8	1.68	46	0.27
	max	0.26	0.36	3.56	25.9	1.92	52	1.39
	mean±SD	0.12±0.07	0.28±0.04	2.66±0.37	24.0±1.2	1.82±0.06	48±	0.64±0.49
	n	16	55	55	17	17	17	5

https://doi.org/10.5194/bg-2022-245
Preprint. Discussion started: 6 January 2023
© Author(s) 2023. CC BY 4.0 License.

Data availability

All datasets on the underway samples (Chlorophyll-a, photophysiology (F_v/F_m and σ_{PSII}) and nutrients (nitrate, phosphate and silicate)), as well as the incubation data which appear in this paper are available on Zenodo <Photophysiological response of autumn phytoplankton in the Antarctic Sea-Ice Zone | Zenodo>; CTD-Rosette surface photophysiology data and the surface iron data from the Go-Flo can also be found at this link. Full datasets for the other CTD-Rosette water column data are available at the Norwegian Polar Data Centre, Norwegian Polar Institute, https://data.npolar.no/dataset (Chlorophyll-a and Mixed Layer Depth) and Norwegian Marine Data Centre, https://doi.org/10.21335/NMDC-1503664923 (nutrients).

Author contributions

TJRK conceptualized the study. AS and TJRK collected the data and performed the data analysis. MVA, NS and AS conducted the trace metal clean water collection and sampling. SM planned the general biological sampling of the cruise. SM and HMK assisted in collecting and analysing the chlorophyll-a data and all the CTD-Rosette samples. SS and AS analysed the dissolved iron samples and SS performed the data analysis and ANR guided the analysis of the dissolved iron samples. AF PI for the SANOCEAN and SOPHY-CO2 project and was involved in cruise planning of the water column sampling onboard the cruise. MC was responsible for water column collection and analyses of all the nutrient samples obtained from the underway, water column and incubation experiments. TNM supported preparations for the iron addition incubations. AS and TJRK produced the figures. AS wrote the initial manuscript. TJRK, SF, SJT and AS contributed to the study design, interpretation of the results and writing of the manuscript. All authors contributed to commenting on the manuscript.

Competing interests

The authors declare that they have no conflict of interest.

Acknowledgements

We would like to acknowledge the support and assistance of the captain and crew of the R/V Kronprins Haakon, along with all the participants on the DML2019702 Ecosystem research cruise. Thank you to Agneta Fransson (NPI) and Sandy Thomalla (CSIR) as the PIs of the SANOCEAN project SOPHY-CO2.

© Author(s) 2023. CC BY 4.0 License.

Financial support

The research expedition, Dronning Maud Land Ecosystem cruise 2019, and the research conducted on the RV Kronprins Haakon were part of a South African – Norwegian collaboration (SANOCEAN SOPHY-CO2), funded by the National Research Foundation (NRF), South Africa (grant UID 118715); the Research Council of Norway (RCN) project number 288370; the Norwegian Polar Institute (NPI), as well as additional financial support from the Norwegian Ministry of Foreign Affairs. AS, SJT and TJRK were supported through the CSIR's Southern Ocean and Carbon Climate Observatory (SOCCO) Programme (http://socco.org.za/) funded by the Department of Science and Innovation (DST/CON 0182/2017) and the CSIR's Parliamentary Grant. We would like to acknowledge funding received from a number of grants from the National Research Foundation, South Africa, grant numbers 110731 (SF), 91313 (SF), 118751 (SJT) and 110729 (SJT).

References

Ardyna, M., Lacour, L., Sergi, S., D'Ovidio, F., Sallée, J.B., Rembauville, M., Blain, S., Tagliabue, A., Schlitzer, R., Jeandel, C., and Arrigo, K.R.: Hydrothermal vents trigger massive phytoplankton blooms in the Southern Ocean. Nat. Commun. 10, 1–8. https://doi.org/10.1038/s41467-019-09973-6, 2019.

Behrenfeld, M.J., and Milligan, A.J.: Photophysiological Expressions of Iron Stress in Phytoplankton. Ann. Rev. Mar. Sci. 5, 217–246. https://doi.org/10.1146/annurev-marine-121211-172356, 2013.

Biggs, T.E., Huisman, J., and Brussaard, C.P.: Viral lysis modifies seasonal phytoplankton dynamics and carbon flow in the Southern Ocean. ISME J. 1–8. https://doi.org/10.1038/s41396-021-01033-6, 2021.

Blain, S., Sarthou, G., and Laan, P.: Distribution of dissolved iron during the natural iron-fertilization experiment KEOPS (Kerguelen Plateau, Southern Ocean). Deep Sea Res. Part II Top. Stud. Oceanogr. 55, 594–605. https://doi.org/10.1016/j.dsr2.2007.12.028, 2008.

Bowie, A.R., Lannuzel, D., Remenyi, T.A., Wagener, T., Lam, P.J., Boyd, P.W., Guieu, C., Townsend, A.T., and Trull, T.W.: Biogeochemical iron budgets of the Southern Ocean south of Australia: Decoupling of iron and nutrient cycles in the subantarctic zone by the summertime supply. Global Biogeochem. Cycles 23, 1–14. https://doi.org/10.1029/2009GB003500, 2009.

Boyd, P.W., and Abraham, E.R.: Iron-mediated changes in phytoplankton photosynthesic competence during SOIREE. Deep. Res. II, Topical Studies in Oceanography, 48(11-12), 2529–2550. https://doi.org/10.1016/S0967-0645(01)00007-8, 2001.

Boyd, P.W., Arrigo, K.R., Strzepek, R., and Van Dijken, G.L.: Mapping phytoplankton iron utilization: Insights into Southern Ocean supply mechanisms. J. Geophys. Res. Ocean. 117, 1–18. https://doi.org/10.1029/2011JC007726, 2012.

Boyd, P.W., and Ellwood, M.J.: The biogeochemical cycle of iron in the ocean. Nat. Geosci. 3, 675–682. https://doi.org/10.1038/ngeo964, 2010.

Boyd, P.W., Jickells, T., Law, C.S., Blain, S., Boyle, E.A., Buesseler, K.O., Coale, K.H., Cullen, J.J., de Baar, H.J.W., Follows, M., Harvey, M., Lancelot, C., Levasseur, M., Owens, N.P.J., Pollard, R., Rivkin, R.B., Sarmiento, J., Schoemann, V., Smetacek, V., Takeda, S., Tsuda, A., Turner, S., and Watson, A.J.: Mesoscale Iron Enrichment Experiments 1993-2005: Synthesis and Future Directions. Science. 315, 612–617. https://doi.org/10.1126/science.1131669, 2007.

Boyd, P.W., Strzepek, R., Fu, F., and Hutchins, D.A.: Environmental control of open-ocean phytoplankton groups: Now and in the future. Limnol. Oceanogr. 55, 1353–1376. https://doi.org/10.4319/lo.2010.55.3.1353, 2010.

Browning, T.J., Achterberg, E.P., Engel, A., and Mawji, E.: Manganese co-limitation of phytoplankton growth and major nutrient drawdown in the Southern Ocean. Nat. Commun. 12, 1–9. https://doi.org/10.1038/s41467-021-21122-6, 2021.

Browning, T.J., Bouman, H.A., Moore, C.M., Schlosser, C., Tarran, G.A., Woodward, E.M.S., and Henderson, G.M.: Nutrient regimes control phytoplankton ecophysiology in the South Atlantic. Biogeosciences 11, 463–479. https://doi.org/10.5194/bg-11-463-2014, 2014a.

Browning, T.J., Bouman, H.A., Henderson, G.M., Mather, T.A., Pyle, D.M., Schlosser, C., Woodward, E.M.S. and Moore, C.M.: Strong responses of Southern Ocean phytoplankton communities to volcanic ash. Geophysical Research Letters, 41(8), 2851-2857. https://doi.org/10.1002/2014GL059364, 2014b.

Chierici, M., and Fransson, A.: Nutrient data (nitrate, phosphate and silicate) in the eastern Weddell gyre, Kong Haakon VII Hav, and the coast of Dronning Maud Land in the Atlantic sector of the Southern Ocean in March 2019, Norwegian Marine Data Centre [data set]. https://doi.org/10.21335/NMDC-1503664923, 2020.

Coale, K.H., Worsfold, P., and de Baar, H.: Iron age in oceanography. Eos, Trans. Am. Geophys. Union 80, 377–382. https://doi.org/10.1029/EO080i034p00377-02, 1999.

Cochlan, W.P.: Nitrogen uptake in the Southern Ocean. Nitrogen in the Marine Environment, 2nd ed. Academic Press, Elsevier. https://doi.org/0.1016/B978-0-12-372522-6.00012-8, 2008.

Cullen, J.J., and Davis, R.F.: The Blank can Make a Big Difference in Oceanographic Measurements. Limnol. Oceanogr. Bull. 12, 29–35. https://doi.org/10.1002/lob.200413229, 2003.

Cutter, G., Casciotti, K., Croot, P., Geibert, W., Heimbürger, L.-E., Lohan, M., Van De Flierdt, T., and Planquette, H.: Sampling and sample-handling protocols for GEOTRACES Cruises Version 3. http://dx.doi.org/10.25607/OBP-2, 2017.

de Baar, H.J.., Buma, A.G.., Nolting, R.., Cadee, G.., Jacques, G., and Treguer, P.: On iron limitation of the Southern Ocean: experimental observations in the Weddell and Scotia Seas. Mar. Ecol. Prog. Ser. 65, 105–122. https://doi.org/10.3354/meps065105, 1990.

de Baar, H.J.W., Boyd, P.W., Coale, K.H., Landry, M.R., Tsuda, A., Assmy, P., Bakker, D.C.E., Bozec, Y., Barber, R.T., Brzezinski, M.A., Buesseler, K.O., Boyé, M., Croot, P.L., Gervais, F., Gorbunov, M.Y., Harrison, P.J., Hiscock, W.T., Laan, P., Lancelot, C., Law, C.S., Levasseur, M., Marchetti, A., Millero, F.J., Nishioka, J., Nojiri, Y., van

Oijen, T., Riebesell, U., Rijkenberg, M.J.A., Saito, H., Takeda, S., Timmermans, K.R., Veldhuis, M.J.W., Waite, A.M., and Wong, C.S.: Synthesis of iron fertilization experiments: From the iron age in the age of enlightenment. J. Geophys. Res. C Ocean. 110, 1–24. https://doi.org/10.1029/2004JC002601, 2005.

Deppeler, S.L., and Davidson, A.T.: Southern Ocean Phytoplankton in a Changing Climate. Front. Mar. Sci. 4, 40. https://doi.org/10.3389/fmars.2017.00040, 2017.

ETOPO1, Global 1 Arc-minute Ocean Depth and Land Elevation From the US National Geophysical Data Center (NGDC): Natl. Geophys. Data Center/NESDIS/NOAA/US Dep. Commer. [URL: https://rda.ucar.edu/datasets/ds759.4/index.html#!description], 2011.

Geider, R.J.: Quantitative phytoplankton physiology: implications for primary production and phytoplankton growth. ICES mar. Sei. Symp 197, 52–62, 1993.

Geider, R.J., and La Roche, J.: The role of iron in phytoplankton photosynthesis, and the potential for iron-limitation of primary productivity in the sea. Photosynth. Res. 39, 275–301. https://doi.org/10.1007/BF00014588, 1994.

Grasshoff, K., Kremling, K., and Ehrhardt, M.: Methods of Seawater Analysis, 3rd ed. Hoboken, NJ: Wiley-VCH. ISBN: 978-3-527-61399-1, 2009.

Hauck, J., Völker, C., Wolf-Gladrow, D.A., Laufkötter, C., Vogt, M., Aumont, O., Bopp, L., Buitenhuis, E.T., Doney, S.C., Dunne, J., and Gruber, N.: On the Southern Ocean CO2 uptake and the role of the biological carbon pump in the 21st century. Global Biogeochem. Cycles 29, 1451–1470. https://doi.org/10.1002/2015GB005140, 2015.

Hinz, D.J., Nielsdóttir, M.C., Korb, R.E., Whitehouse, M.J., Poulton, A.J., Moore, C.M., Achterberg, E.P., and Bibby, T.S.: Responses of microplankton community structure to iron addition in the Scotia Sea. Deep. Res. Part II Top. Stud. Oceanogr. 59–60, 36–46. https://doi.org/10.1016/j.dsr2.2011.08.006, 2012.

Hiscock, M.R., Lance, V.P., Apprill, A.M., Bidigare, R.R., Johnson, Z.I., Mitchell, B.G., Smith, W.O., and Barber, R.T.: Photosynthetic maximum quantum yield increases are an essential component of the Southern Ocean phytoplankton response to iron. Proc. Natl. Acad. Sci. 105, 4775–4780. https://doi.org/10.1073/pnas.0705006105, 2008.

Holm-Hansen, O., and Riemann, B.: Chlorophyll a Determination : Improvements in Methodology. Wiley on behalf of Nordic Society Oikos. http://www.jstor.org/stable/3543338, 1978.

Hughes, D.J., Campbell, D.A., Doblin, M.A., Kromkamp, J.C., Lawrenz, E., Moore, C.M., Oxborough, K., Prášil, O., Ralph, P.J., Alvarez, M.F., and Suggett, D.J.: Roadmaps and Detours: Active Chlorophyll- a Assessments of Primary Productivity Across Marine and Freshwater Systems. Environ. Sci. Technol. 52, 12039–12054. https://doi.org/10.1021/acs.est.8b03488, 2018.

Kauko, H.M., Hattermann, T., Ryan-Keogh, T., Singh, A., de Steur, L., Fransson, A., Chierici, M., Falkenhaug, T., Hallfredsson, E.H., Bratbak, G., and Tsagaraki, T.: Phenology and environmental control of phytoplankton blooms in the Kong Håkon VII Hav in the Southern Ocean. Front. Mar. Sci. 8, 287. https://doi.org/10.3389/fmars.2021.623856, 2021.

Kauko, H. M., Moreau, S., Rózañska, M., and Wiktor, J. M.: Southern Ocean Ecosystem cruise 2019 phytoplankton taxonomy and abundance, Norwegian Polar Institute [data set]. https://doi.org/10.21334/npolar.2022.283e500c, 2022a.

Kauko, H.M., Assmy, P., Peeken, I., Różańska-Pluta, M., Wiktor, J.M., Bratbak, G., Singh, A., Ryan-Keogh, T.J., and Moreau, S.: First phytoplankton community assessment of the Kong Håkon VII Hav, Southern Ocean, during austral autumn, Biogeosciences, 19, 5449–5482. https://doi.org/10.5194/bg-19-5449-2022, 2022b.

Kauko, H. M., Moreau, S., and Hattermann, T.: Southern Ocean Ecosystem cruise 2019 vertical in situ chlorophyll a profiles, Norwegian Polar Institute [data set]. https://doi.org/10.21334/npolar.2021.5e510f85, 2020.

Khatiwala, S., Primeau, F., and Hall, T.: Reconstruction of the history of anthropogenic CO2 concentrations in the ocean. Nature 462, 346–349. https://doi.org/10.1038/nature08526, 2009.

Kirk, J.T.O.: Light and photosynthesis in aquatic ecosystems. Cambridge university press. https://doi.org/10.1017/CBO9780511623370, 1994.

Klunder, M.B., Laan, P., Middag, R., De Baar, H.J.W., and van Ooijen, J.C.: Dissolved iron in the Southern Ocean (Atlantic sector). Deep. Res. Part II Top. Stud. Oceanogr. 58, 2678–2694. https://doi.org/10.1016/j.dsr2.2010.10.042, 2011.

Kolber, Z., Zehr, J., and Falkowski, P.: Effects of Growth Irradiance and Nitrogen Limitation on Photosynthetic Energy Conversion in Photosystem II. Plant Physiol. 88, 923–929. https://doi.org/10.1104/pp.88.3.923, 1988.

Kolber, Z.S., Barber, R.T., Coale, K.H., Fitzwateri, S.E., Greene, R.M., Johnson, K.S., Lindley, S., and Falkowski, P.G.: Iron limitation of phytoplankton photosynthesis in the equatorial Pacific Ocean. Nature 371, 145–149. https://doi.org/10.1038/371145a0, 1994.

Kolber, Z.S., Prášil, O., and Falkowski, P.G.: Measurements of variable chlorophyll fluorescence using fast repetition rate techniques: defining methodology and experimental protocols. Biochim. Biophys. Acta - Bioenerg. 1367, 88–106. https://doi.org/10.1016/S0005-2728(98)00135-2, 1998.

Lancelot, C., Mathot, S., Veth, C., and de Baar, H.: Factors controlling phytoplankton ice-edge blooms in the marginal ice-zone of the northwestern Weddell Sea during sea ice retreat 1988: field observations and mathematical modelling. Polar Biol. 13, 377–387. https://doi.org/10.1007/BF01681979, 1993.

Lannuzel, D., Schoemann, V., de Jong, J., Chou, L., Delille, B., Becquevort, S., and Tison, J.L.: Iron study during a time series in the western Weddell pack ice. Mar. Chem. 108, 85–95. https://doi.org/10.1016/j.marchem.2007.10.006, 2008.

Lindsey, R. and Scott, M.: What are Phytoplankton? [URL: https://earthobservatory.nasa.gov/Features/Phytoplankton/printall.php] (accessed 11.8.17), 2010.

Lucas, M., Seeyave, S., Sanders, R., Moore, C.M., Williamson, R., and Stinchcombe, M.: Nitrogen uptake responses to a naturally Fe-fertilised phytoplankton bloom during the 2004/2005 CROZEX study. Deep Sea Res. Part II Top. Stud. Oceanogr. 54, 2138–2173. https://doi.org/10.1016/j.dsr2.2007.06.017, 2007.

Lutjeharms, J.R.E., Walters, N.M., and Allanson, B.R.: Oceanic frontal systems and biological enhancement, in: Antarctic Nutrient Cycles and Food Webs. Springer Berlin Heidelberg, pp. 11–21. https://doi.org/10.1007/978-3-642-82275-9_3, 1985.

Mahowald, N.M., Baker, A.R., Bergametti, G., Brooks, N., Duce, R.A., Jickells, T.D., Kubilay, N., Prospero, J.M., and Tegen, I..: Atmospheric global dust cycle and iron inputs to the ocean. Global Biogeochem. Cycles 19. https://doi.org/10.1029/2004GB002402, 2005.

Martin, J.H., and Fitzwater, S.E.: Iron deficiency limits phytoplankton growth in the north-east Pacific subarctic. Nature 331, 341–343. https://doi.org/10.1038/331341a0, 1988.

Martin, J.H., Gordon, M., and Fitzwater, S.E.: The case for iron. Limnol. Oceanogr. 36, 1793–1802. https://doi.org/10.4319/lo.1991.36.8.1793, 1991.

Martin, J.H., Gordon, R.M., and Fitzwater, S.E.: Iron in Antarctic waters. Nature 345, 156–158. https://doi.org/10.1038/345156a0, 1990.

Millard, R. C., Owens, W. B. & Fofonoff, N. P.: On the calculation of the Brunt-Väisäla frequency. Deep Sea Res. Part A. Oceanogr. Res. Pap. 37, 167–181. https://doi.org/10.1016/0198-0149(90)90035-T, 1990.

Milligan, A.J., and Harrison, P.J.: Effects of non-steady-state iron limitation on nitrogen assimilatory enzymes in the marine diatom thalassiosira weissflogii (BACILLARIOPHYCEAE). J. Phycol. 36, 78–86. https://doi.org/10.1046/j.1529-8817.2000.99013.x, 2000.

Mitchell, B.G., Brody, E.A., Holm-Hansen, O., McClain, C., and Bishop, J.: Light limitation of phytoplankton biomass and macronutrient utilization in the Southern Ocean. Limnol. Oceanogr. 36, 1662–1677. https://doi.org/10.4319/lo.1991.36.8.1662, 1991.

Moore, C.M., Hickman, A.E., Poulton, A.J., Seeyave, S., and Lucas, M.I.: Iron – light interactions during the CROZet natural iron bloom and EXport experiment (CROZEX): II – Taxonomic responses and elemental stoichiometry 54, 2066–2084. https://doi.org/10.1016/j.dsr2.2007.06.015, 2007a.

Moore, C.M., Mills, M.M., Arrigo, K.R., Berman-Frank, I., Bopp, L., Boyd, P.W., Galbraith, E.D., Geider, R.J., Guieu, C., Jaccard, S.L., Jickells, T.D., La Roche, J., Lenton, T.M., Mahowald, N.M., Marañón, E., Marinov, I., Moore, J.K., Nakatsuka, T., Oschlies, A., Saito, M.A., Thingstad, T.F., Tsuda, A., and Ulloa, O.: Processes and patterns of oceanic nutrient limitation. Nat. Geosci. 6, 701–710. https://doi.org/10.1038/ngeo1765, 2013.

Moore, C.M., Seeyave, S., Hickman, A.E., Allen, J.T., Lucas, M.I., Planquette, H., Pollard, R.T., and Poulton, A.J.: Iron-light interactions during the CROZet natural iron bloom and EXport experiment (CROZEX) I: Phytoplankton growth and photophysiology. Deep. Res. Part II Top. Stud. Oceanogr. 54, 2045–2065. https://doi.org/10.1016/j.dsr2.2007.06.011, 2007b.

Moore, J.K., and Abbott, M.R.: Surface chlorophyll concentrations in relation to the Antarctic Polar Front: seasonal and spatial patterns from satellite observations. J. Mar. Syst. 37, 69–86. https://doi.org/10.1016/S0924-7963(02)00196-3, 2002.

Moreau, S., Boyd, P.W., and Strutton, P.G.: Remote assessment of the fate of phytoplankton in the Southern Ocean sea-ice zone. Nat. Commun. 11, 1–9. https://doi.org/10.1038/s41467-020-16931-0, 2020.

Mtshali, T.N., van Horsten, N.R., Thomalla, S.J., Ryan-Keogh, T.J., Nicholson, S.A., Roychoudhury, A.N., Bucciarelli, E., Sarthou, G., Tagliabue, A., and Monteiro, P.M.S.: Seasonal Depletion of the Dissolved Iron Reservoirs in the Sub-Antarctic Zone of the Southern Atlantic Ocean. Geophys. Res. Lett. 46, 4386–4395. https://doi.org/10.1029/2018GL081355, 2019.

Nicholson, S.-A., Lévy, M., Jouanno, J., Capet, X., Swart, S., and Monteiro, P.M.S.: Iron Supply Pathways Between the Surface and Subsurface Waters of the Southern Ocean: From Winter Entrainment to Summer Storms. Geophys. Res. Lett. Am. Geophys. Union 46, 14567–14575. https://doi.org/10.1029/2019GL084657, 2019.

Pollard, R., Sanders, R., Lucas, M., and Statham, P.: The Crozet Natural Iron Bloom and Export Experiment (CROZEX). Deep. Res. Part II Top. Stud. Oceanogr. 54, 1905–1914. https://doi.org/10.1016/j.dsr2.2007.07.023, 2007.

Price, N.M., Ahner, B.A., and Morel, F.M.: The equatorial Pacific Ocean: Grazer-controlled phytoplankton populations in an iron-limited ecosystem 1. Limnol. Oceanogr. 39, 520–534. https://doi.org/10.4319/LO.1994.39.3.0520, 1994.

Racault, M.F., Sathyendranath, S., and Platt, T.: Impact of missing data on the estimation of ecological indicators from satellite ocean-colour time-series. Remote Sens. Environ. 152, 15–28. https://doi.org/10.1016/j.rse.2014.05.016, 2014.

Raven, J.A.: Predictions of Mn and Fe use efficiencies of phototrophic growth as a function of light availability for growth and of C assimilation pathway. New Phytol. 116, 1–18. https://doi.org/10.1111/j.1469-8137.1990.tb00505.x, 1990.

Raven, J.A., Evans, M.C.W., and Korb, R.E.: The role of trace metals in photosynthetic electron transport in O-2-evolving organisms. Photosynth. Res. 60, 111–149. https://doi.org/10.1023/a:1006282714942, 1999.

Richert, I., Yager, P.L., Dinasquet, J., Logares, R., Riemann, L., Wendeberg, A., Bertilsson, S., and Scofield, D.G.: Summer comes to the Southern Ocean: how phytoplankton shape bacterioplankton communities far into the deep dark sea. Ecosphere 10, e02641. https://doi.org/10.1002/ecs2.2641, 2019.

Roháček, K.: Chlorophyll fluorescence parameters: The definitions, photosynthetic meaning, and mutual relationships. Photosynthetica. https://doi.org/10.1023/A:1020125719386, 2002.

Ryan-Keogh, T.J., and Robinson, C.: Phytoplankton Photophysiology Utilities: A Python Toolbox for the Standardization of Processing Active Chlorophyll-a Fluorescence Data. Front. Mar. Sci. Aquat. Physiol. 8, 526. https://doi.org/10.3389/fmars.2021.525414, 2021.

Ryan-Keogh, T.J.: Understanding the role of chlorophyll fluorescence in nutrient stress. University of Southampton. http://eprints.soton.ac.uk/id/eprint/362003, 2014.

Ryan-Keogh, T.J., DeLizo, L.M., Smith, W.O., Sedwick, P.N., McGillicuddy, D.J., Moore, C.M., and Bibby, T.S.: Temporal progression of photosynthetic-strategy in phytoplankton in the Ross Sea, Antarctica. J. Mar. Syst. 166, 87–96. https://doi.org/10.1016/j.jmarsys.2016.08.014, 2017a.

© Author(s) 2023. CC BY 4.0 License.

Ryan-Keogh, T.J., Macey, A.I., Nielsdóttir, M.C., Lucas, M.I., Steigenberger, S.S., Stinchcombe, M.C., Achterberg, E.P., Bibby, T.S., and Moore, C.M.: Spatial and temporal development of phytoplankton iron stress in relation to bloom dynamics in the high-latitude North Atlantic Ocean. Limnol. Oceanogr. 58, 533–545. https://doi.org/10.4319/lo.2013.58.2.0533, 2013.

Ryan-Keogh, T.J., Thomalla, S.J., Mtshali, T.N., and Little, H.: Modelled estimates of spatial variability of iron stress in the Atlantic sector of the Southern Ocean. Biogeosciences 14, 3883–3897. https://doi.org/10.5194/bg-14-3883-2017, 2017b.

Ryan-Keogh, T.J., Thomalla, S.J., Mtshali, T.N., Van Horsten, N.R., and Little, H.J.: Seasonal development of iron limitation in the sub-Antarctic zone. Biogeosciences 15, 4647–4660. https://doi.org/10.5194/bg-15-4647-2018, 2018.

Salgado-Hernanz, P.M., Racault, M.F., Font-Muñoz, J.S., and Basterretxea, G.: Trends in phytoplankton phenology in the Mediterranean Sea based on ocean-colour remote sensing. Remote Sens. Environ. 221, 50–64. https://doi.org/10.1016/j.rse.2018.10.036, 2019.

Samanta, S., Cloete, R., Loock, J., Rossouw, R., and Roychoudhury, A.N.: Determination of trace metal (Mn, Fe, Ni, Cu, Zn, Co, Cd and Pb) concentrations in seawater using single quadrupole ICP-MS: A comparison between offline and online preconcentration setups. Minerals 11, 1289. https://doi.org/10.3390/min11111289, 2021.

Sathyendranath, S., Brewin, R.J., Brockmann, C., Brotas, V., Calton, B., Chuprin, A., Cipollini, P., Couto, A.B., Dingle, J., Doerffer, R., and Donlon, C.: An ocean-colour time series for use in climate studies: the experience of the ocean-colour climate change initiative (OC-CCI). Sensors 19, 4285. https://doi.org/10.3390/s19194285, 2019.

Schuback, N., Flecken, M., Maldonado, M.T. and Tortell, P.D.: Diurnal variation in the coupling of photosynthetic electron transport and carbon fixation in iron-limited phytoplankton in the NE subarctic Pacific. Biogeosciences, 13(4), 1019-1035. https://doi.org/10.5194/bg-13-1019-2016, 2016.

Sedwick, P.N., Bowie, A.R., and Trull, T.W.: Dissolved iron in the Australian sector of the Southern Ocean (CLIVAR SR3 section): meridional and seasonal trends. Deep Sea Res. I Ocean. Res. Pap. 55, 911–925. https://doi.org/10.1016/j.dsr.2008.03.011, 2008.

Sedwick, P.N., DiTullio, G.R., Hutchins, D.A., Boyd, P.W., Griffiths, F.B., Crossley, A.C., Trull, T.W. and Quéguiner, B.: Limitation of algal growth by iron deficiency in the Australian Subantarctic region. Geophysical Research Letters, 26(18), 2865-2868. https://doi.org/10.1029/1998GL002284, 1999.

Singh, A., Fietz, S., Thomalla, S.J., Sanchez, N., Ardelan, M.V., Moreau, S., Kauko, H.M., Fransson, A., Chierici, M., Samanta, S., Mtshali, T.N., Roychoudhury, A.N., and Ryan-Keogh, T. J.: Photophysiological response of autumn phytoplankton in the Antarctic Sea-Ice Zone [data set]. Zenodo. https://doi.org/10.5281/zenodo.6322943, 2022.

Smith, W.O., Dinniman, M.S., Tozzi, S., DiTullio, G.R., Mangoni, O., Modigh, M., and Saggiomo, V.: Phytoplankton photosynthetic pigments in the Ross Sea: Patterns and relationships among functional groups. J. Mar. Syst. 82, 177–185. https://doi.org/10.1016/j.jmarsys.2010.04.014, 2010.

Soppa, M.A., Völker, C., and Bracher, A.: Diatom phenology in the Southern Ocean: mean patterns, trends and the role of climate oscillations. Remote Sens. 8, 420. https://doi.org/10.3390/rs8050420, 2016.

Strzepek, R.F., Boyd, P.W., and Sunda, W.G.: Photosynthetic adaptation to low iron, light, and temperature in Southern Ocean phytoplankton. Proc. Natl. Acad. Sci. 116, 4388–4393. https://doi.org/10.1073/pnas.1810886116, 2019.

Strzepek, R.F., and Harrison, P.J.: Photosynthetic architecture differs in coastal and oceanic diatoms. Nature 431, 689–692. https://doi.org/10.1038/nature02954, 2004.

Strzepek, R.F., Hunter, K.A., Frew, R.D., Harrison, P.J., and Boyd, P.W.: Iron-light interactions differ in Southern Ocean phytoplankton. Limnol. Oceanogr. 57, 1182–1200. https://doi.org/10.4319/lo.2012.57.4.1182, 2012.

Strzepek, R.F., Maldonado, M.T., Hunter, K.A., Frew, R.D., and Boyd, P.W.: Adaptive strategies by Southern Ocean phytoplankton to lessen iron limitation: Uptake of organically complexed iron and reduced cellular iron requirements. Limnol. Oceanogr. 56, 1983–2002. https://doi.org/10.4319/lo.2011.56.6.1983, 2011.

Suggett, D., Kraay, G., Holligan, P., Davey, M., Aiken, J., and Geider, R.: Assessment of photosynthesis in a spring cyanobacterial bloom by use of a fast repetition rate fluorometer. Limnol. Oceanogr. 46, 802–810. https://doi.org/10.4319/lo.2001.46.4.0802, 2001.

Suggett, D.J., Moore, C.M., Hickman, A.E., and Geider, R.J.: Interpretation of fast repetition rate (FRR) fluorescence: Signatures of phytoplankton community structure versus physiological state. Mar. Ecol. Prog. Ser. 376, 1–19. https://doi.org/10.3354/meps07830, 2009.

Sunda, W.G.: Trace metal interactions with marine phytoplankton. Biol. Oceanogr. 6, 411–442, 1989.

Sunda, W.G., and Huntsman, S.A.: Interrelated influence of iron, light and cell size on marine phytoplankton growth. Nature 390, 389–392. https://doi.org/10.1038/37093, 1997.

Sunda, W.G., and Huntsman, S.A.: Iron uptake and growth limitation in oceanic and coastal phytoplankton. Mar. Chem. 50, 189–206. https://doi.org/10.1016/0304-4203(95)00035-P, 1995.

Swart, S., Thomalla, S.J., and Monteiro, P.M.S.: The seasonal cycle of mixed layer dynamics and phytoplankton biomass in the Sub-Antarctic Zone: A high-resolution glider experiment. J. Mar. Syst. 147, 103–115. https://doi.org/10.1016/j.jmarsys.2014.06.002, 2015.

Tagliabue, A., Bowie, A.R., Boyd, P.W., Buck, K.N., Johnson, K.S., and Saito, M.A.: The integral role of iron in ocean biogeochemistry. Nature 543, 51–59. https://doi.org/10.1038/nature21058, 2017.

Tagliabue, A., Sallée, J.B., Bowie, A.R., Lévy, M., Swart, S., and Boyd, P.W.: Surface-water iron supplies in the Southern Ocean sustained by deep winter mixing. Nat. Geosci. 7, 314–320. https://doi.org/10.1038/ngeo2101, 2014.

Takahashi, T., Sutherland, S.C., Sweeney, C., Poisson, A., Metzl, N., Tilbrook, B., Bates, N., Wanninkhof, R., Feely, R.A., Sabine, C., Olafsson, J., and Yukihiro, N.: Global sea–air CO2 flux based on climatological surface ocean pCO2, and seasonal biological and temperature effects. Deep Sea Res. Part II Top. Stud. Oceanogr. 49, 1601–1622. https://doi.org/10.1016/S0967-0645(02)00003-6, 2002.

https://doi.org/10.5194/bg-2022-245
Preprint. Discussion started: 6 January 2023
© Author(s) 2023. CC BY 4.0 License.

Takahashi, T., Sutherland, S.C., Wanninkhof, R., Sweeney, C., Feely, R.A., Chipman, D.W., Hales, B., Friederich, G., Chavez, F., Sabine, C., and Watson, A.: Climatological mean and decadal change in surface ocean pCO2, and net sea–air CO2 flux over the global oceans. Deep Sea Res. Part II Top. Stud. Oceanogr. 56, 554–577. https://doi.org/10.1016/j.dsr2.2008.12.009, 2009.

Taylor, M.H., Losch, M., Bracher, A.: On the drivers of phytoplankton blooms in the Antarctic marginal ice zone: A modeling approach. J. Geophys. Res. Ocean. 118, 63–75. https://doi.org/10.1029/2012JC008418, 2013.

Van Oijen, T., Van Leeuwe, M.A., Granum, E., Weissing, F.J., Bellerby, R.G.J., Gieskes, W.W.C., and de Baar, H.J.W.: Light rather than iron controls photosynthate production and allocation in Southern Ocean phytoplankton populations during austral autumn. J. Plankton Res. 26, 885–900. https://doi.org/10.1093/plankt/fbh088, 2004.

Viljoen, J.J., Philibert, R., Van Horsten, N., Mtshali, T., Roychoudhury, A.N., Thomalla, S., and Fietz, S.: Phytoplankton response in growth, photophysiology and community structure to iron and light in the Polar Frontal Zone and Antarctic waters. Deep Sea Res. Part I Oceanogr. Res. Pap. 141, 118–129. https://doi.org/10.2495/EEIA100071, 2018.

Vink, S., and Measures, C.I.: The role of dust deposition in determining surface water distributions of Al and Fe in the South West Atlantic. Deep Sea Res. Part II Top. Stud. Oceanogr. 48, 2787–2809. https://doi.org/10.1016/S0967-0645(01)00018-2, 2001.